THE PERFORMANCE OF ITERATIVELY REWEIGHTED MULTIVARIATE ALTERATION DETECTION (IRMAD) APPLIED ON UNTRANSFORMED AND TRANSFORMED LANDSAT SURFACE REFLECTANCE

Dyah R. Panuju[1, 2], David J. Paull [1], Amy L. Griffin [1], Bambang H. Trisasongko [1, 2]

[1] School of Physical, Environmental and Mathematical Sciences, UNSW Canberra, Australia
[2] Department of Soil Science and Land Resource, Bogor Agricultural University, Indonesia
Email: dyah.panuju@student.adfa.edu.au; panuju@apps.ipb.ac.id

ABSTRACT: The iteratively reweighted multivariate alteration detection (IRMAD) based on canonical correlation is a popular technique for bi-temporal analysis. We demonstrate its potential to assist in the investigation of historical change of land surfaces in this research. Our particular interest was in how IRMAD performed using different data inputs to detect simultaneous historical change in a heterogeneous topographical region of West Java. This article investigates IRMAD's performance with untransformed and transformed surface reflectance from LANDSAT 5 TM and LANDSAT 8 OLI. Two forms of transformation were studied: tasseled cap transformation, and a set of indices consisting of the Normalised Difference Vegetation Index (NDVI), the Normalised Difference Water Index (NDWI) and the brilliance index (BI), which together contain comparable information to the tasseled cap transformation. We found that canonical correlation stability seems to be reached quickly on transformed data, and consistently on both the tasseled cap transformation and the set of indices. The tasseled cap transformation appears to increase the proportion of variance at the first variate, and results in more accurate change detection compared to the original surface reflectance and the set of indices. We found that the generation of the MAD variates was influenced by the type of sensor and transformations. Landsat TM5 appears to result in a smaller mean and variance of the variates than Landsat OLI. Meanwhile, transformation, i.e. tasselled cap and the set of indices, seems to produce a smaller mean and variance of MAD variates compared to what was generated by original surface reflectance.

KEYWORDS: Change detection, multivariate alteration detection, Landsat, surface reflectance, transformation, tasselled cap, vegetation indices

1. Introduction

A robust technique to identify change is essential for accurate change detection. Either original or transformed surface reflectance can be used for change detection, however limited experiments have been attempted to compare the robustness of these options. Bi-temporal change detection techniques have been developed to assist in monitoring the alteration of the global land surface. Bi-temporal change detection is different from temporal trajectory analysis (Gong et al., 2008) with regard to the frequency of observations and evaluation of the process of change.

The performance of bi-temporal change detection techniques is dictated by several factors, i.e. data selection including the temporal, spatial, spectral and radiometric resolutions of satellite images; environmental conditions, for instance atmospheric, soil and phenological properties; pre-processing; as well as sensitivity of algorithm for the detection (Coppin, 2004). Several strategies have been applied to deal with these obstacles. Selecting anniversary dates of image acquisition is a common strategy (Lunetta et al., 2004) to reduce the effect of seasonal dynamics and sun angle differences for comparison of data pairs (Alaibakhsh et al., 2015). However, this strategy may not be as useful in tropical areas where persistent cloud cover (more than 80%) is common. Utilising the same sensor for paired images for change detection is a common approach to lessen noise that may be imposed when different spectral images are employed. Nonetheless, a long-term study likely requires diverse sensors to allow continuous monitoring due to limited lifetimes of particular sensors. Most authors suggest that pre-processing plays an important role in bi-temporal change detection (Coppin and Bauer, 1996; Son et al., 2016). However, many researchers have concluded that no change detection method provided superior performance across all criteria such as accuracy, or capacity to deal with errors sourced from misregistration or seasonal circumstances (Coppin and Bauer, 1996).

A literature survey shows that methods for bi-temporal change detection can be classified into two groups: post-classification or direct change detection (Singh, 1989). The two groups are also sometimes named classification-based or direct spectral comparison, respectively. Gong et al. (2016) proposed a division of the direct spectral comparison techniques into joint classification detection or simple detection. The identification of change in joint classification is performed by stacking images taken at two or more points in time prior to selecting training samples for the sequence of changes. Simple detection compares spectral values of a pair of images.

The latest technique for bi-temporal change detection, multivariate alteration detection (MAD) and its modification, iteratively reweighted MAD (IRMAD), is based on canonical correlation, which has been shown to be robust for change detection (Nielsen, 2007). MAD has been described as a well-established method for bi-temporal change detection (Marpu et al., 2011) that shows improvements in handling problems such as image registration, spectral

normalization and spatial autocorrelation combined in one technique (Nielsen et al., 1998). MAD has been applied to images from various sensors such as Landsat (Canty and Nielsen, 2008), AVHRR (Schmidt et al., 2008), ASTER (Canty and Nielsen, 2008), and synthetically derived images (Wang et al., 2015). It has also been applied to various ecological conditions, for instance in a coastal ecosystem (Bernardo et al., 2016), forested area (Schroeder et al., 2006), and urban region (Doxani et al., 2012). However, very few, if any reports specifically focus on comparing the technique's performance with transformed and untransformed data or across different sensors to reveal dynamic processes.

This article discusses the application of IRMAD in a heterogeneous topographical region of West Java using the most ingested data, surface reflectance (SR), and transformed SR, i.e. tasselled cap and a set of indices, to enrich our understanding of the advantages and disadvantages of using IRMAD for bi-temporal change detection. It also examines the performance of IRMAD using different Landsat sensors to study historical change.

2. Pre-processing in bi-temporal analysis

Pre-processing is a necessity in bi-temporal analysis to minimise error in detecting changes. Error in change detection may be due to radiometric, geometric and atmospheric differences between two images (Milne, 1988). Geometric correction is carried out to co-register a pair of images and minimise misregistration in order to reduce the detection of spurious changes due to misaligned data pairs. Misregistration has been identified as the biggest source of bias in change detection, contributing more than 50% of errors (Townshend et al., 1992). Several algorithms to co-register data are available and correlation-based techniques have been widely applied for this task (Ayoub et al., 2009; Leprince et al., 2007). The cross-correlation method for co-registration has been criticised as computationally inefficient, but has become popular with advances in computer technology.

Another essential pre-processing step for bi-temporal analysis is image transformation, which allows characterisation of physical properties using fewer spectral images. The transformation converts multispectral images into a smaller number of components with minimum information loss. One spectral volume reduction method is principal component analysis (PCA), which transforms the original data into linear combinations of uncorrelated spectral information (Deng et al., 2008). The technique has been applied to identify change by integrating observations at two time points as a bundle of datasets. The identification of change in PCA is from the generated components having smaller variances. PCA can be efficiently computed, however the derived components present considerable problems with regard to the interpretation of physical features (Crist, 1985).

Tasselled cap (TC) is another type of spectral transformation that also describes the relationships among bands and extracts biophysical characteristics of the channels (Crist and Cicone, 1984; Kauth and Thomas, 1976). TC generates three features that represent brightness, greenness and wetness (Kauth and Thomas, 1976). TC coefficients have been calculated using various sensors, including Landsat TM (Crist and Cicone, 1984), Landsat 7 ETM+ (Huang et al., 2002), Landsat 8 OLI (Baig et al., 2014), and MODIS (Lobser and Cohen, 2007). The applications of TC include the study of plant succession (Fiorella and Ripple, 1993), the development of annual land cover maps (Homer et al., 2004), and the spatio-temporal quantification of urban environments (Seto and Fragkias, 2005). While having the advantages of reducing the number of spectral bands and being easy to relate to biophysical features, TC is reported to be dependent on sensor properties (Crist, 1985).

The most popular transformation technique is forming indices that allow some spectral bands to represent targeted biophysical properties. Vegetation indices, particularly the Normalised Difference Vegetation Index (NDVI), have been the most popular for various applications. The applications include identification of the expansion or shrinkage of vegetated areas such as agriculture (Van Niel and McVicar, 2004), forest (Huete, 2012), and the built-up environment (Gallo and Tarpley, 1996). Other indices include the Normalised Difference Built-up Index (NDBI) which specifically represents impervious surface (Zha et al., 2003); Normalised Difference Water Index (NDWI), used to characterise water areas (McFeeters, 1996); or Land Surface Temperature (LST) to study heat islands (Lambin and Ehrlich, 1997). Comparing a set of indices that are comparable with the TC transformation can demonstrate the potential use of these transformations for change detection.

The normalisation or calibration of multi-temporal images may be another important pre-processing step that is required to reduce the effect of radiometric as well as atmospheric differences on the detection of changes. This pre-processing is argued to be a necessity in bi-temporal change detection, particularly to compensate for differences in sensor gain, between data pairs (Du et al., 2002). Absolute and relative normalisation methods have been developed, and it appears that multivariate alteration detection is the newest technique that has been widely used to perform relative normalisation (Canty and Nielsen, 2008; Schroeder et al., 2006). This technique incorporates the ability to minimise misregistration and to normalise a pair of images to allow continuous comparison within multi- or hyper-

temporal change detection studies. Most applications of the technique have shown that the modified MAD, IRMAD, was robust for relative normalisation (Nielsen, 2007) and generating a map of changes.

3. Multivariate Alteration Detection (MAD) and Iteratively Reweighted MAD (IRMAD)

MAD is frequently used for change detection. The motivation for choosing this technique varied among users, for instance to calibrate two acquisition time points or to analyse and map changes. The method is based on Hotteling's (1936) canonical correlation in which two sets of vector images taken at the same place, acquired at two time points, $M=(M_1, \ldots, M_k)$ and $N=(N_1, \ldots, N_k)$, are transformed into new images $Q= a^T M$ and $R= b^T N$. As suggested by Nielsen et al. (1998), vectors a^T and b^T are selected simultaneously by maximising variance of the difference between Q and R subject to the constraint that the variance of Q and R are both equal to 1,

$$Max[Var(Q-R)], subject\ to\ Var(Q) = Var(R) = 1\ ,$$
$$Var(Q-R) = Var(Q) + Var(R) - 2Cov(Q,R) \quad (1)$$

By maximising the covariance of Q and R, MAD generates variance of [Q-R] to comply canonical correlation analysis. Hence, maximising the difference between Q and R can be achieved by minimising non-negative correlation (ρ):

$$\rho = \frac{Cov(Q,R)}{\sqrt{Var(Q)Var(R)}} \quad (2)$$

The variance of the difference then can be written as Var(Q-R) = 2(1-ρ), where ρ is the correlation between Q and R. The MAD transformation as the change result was defined by Nielsen et al. (1998) as:

$$\begin{bmatrix} M \\ N \end{bmatrix} \Rightarrow \begin{bmatrix} a_p^T M & - & b_p^T N \\ \vdots & \ddots & \vdots \\ a_1^T M & - & b_1^T N \end{bmatrix} \quad (3)$$

From p spectral bands in the original images, two images can be generated where each new image is composed of p MAD-variates. The MAD-variates are orthogonal to each other and are ordered by descending variance. To deal with different scales due to different gain factors and atmospheric conditions, standardising values by computing their correlation instead of their covariance, was suggested. IRMAD's iterative processing is performed to improve separation among classes by adding more weight to no-change probabilities during the process (Nielsen, 2007).

Land surface dynamics in tropical regions have been studied by applying IRMAD to images from various Landsat sensors in order to explore the historical change processes in the area. As the longest time series of regional scale data available for change analysis, several Landsat sensors have been operable, providing continuous monitoring of the land surface beginning with MSS, then TM and OLI. These sensors are indispensable to supporting long-term monitoring at medium spatial resolution, which allows characterisation of causes of change. Alaibakhsh et al. (2015) applied IRMAD to characterise change processes using a series of Landsat images spanning more than a decade, validated by time series of multi-temporal indices derived from the same sensor.

4. Materials and Methods

4.1. Images and Ancillary Data

Landsat TM5 path 122, row 65 from five time points Julian dated 273, 273, 210, 210, and 173 for the respective years 1991, 1997, 2000, 2006, 2007 were employed (see Figure 1). Additionally, Landsat 8 OLI of the same path/rows on the Julian dates 173 and 221 in 2013 and 2016, respectively, were used to allow the comparison of bi-temporal change detection using different Landsat sensors and different transformation approaches. Landsat surface reflectance at those time points was employed to analyse change. The surface reflectance data were atmospherically and geometrically corrected images generated by using the United States Geological Survey's (USGS) Landsat Ecosystem Disturbance Adaptive Processing System (LEDAPS). This product is considered provisional and is specifically designed to support land change studies. Interested readers should refer to Liang et al. (2001) for a full description of the concept behind the program and the pre-processing algorithm.

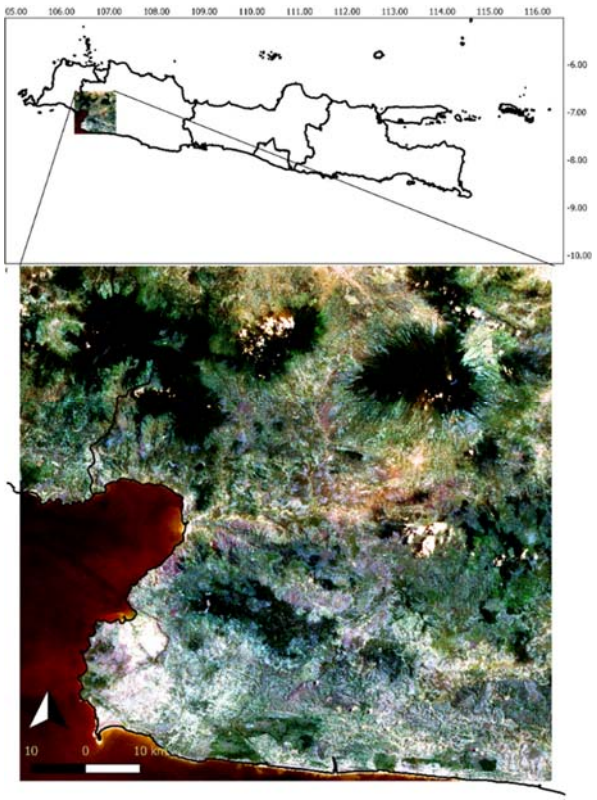

Figure 1. Example of Landsat images used in the experiment. The image is an RGB 1-2-3 of Landsat Path 122 Row 65 acquired at Julian date 1997257 (14 September 1997).

4.2. Methods

In general, the experiment was initially performed by reprojecting, sub-setting, and concatenating multispectral images of surface reflectance provided by the USGS. The transformation of surface reflectance was followed by IRMAD analyses of the transformation products and the original surface reflectance. The process produced MAD variates, mean and standard deviation of change distribution, and a map of detected changes for evaluation. The general procedure of the process is illustrated in Figure 2.

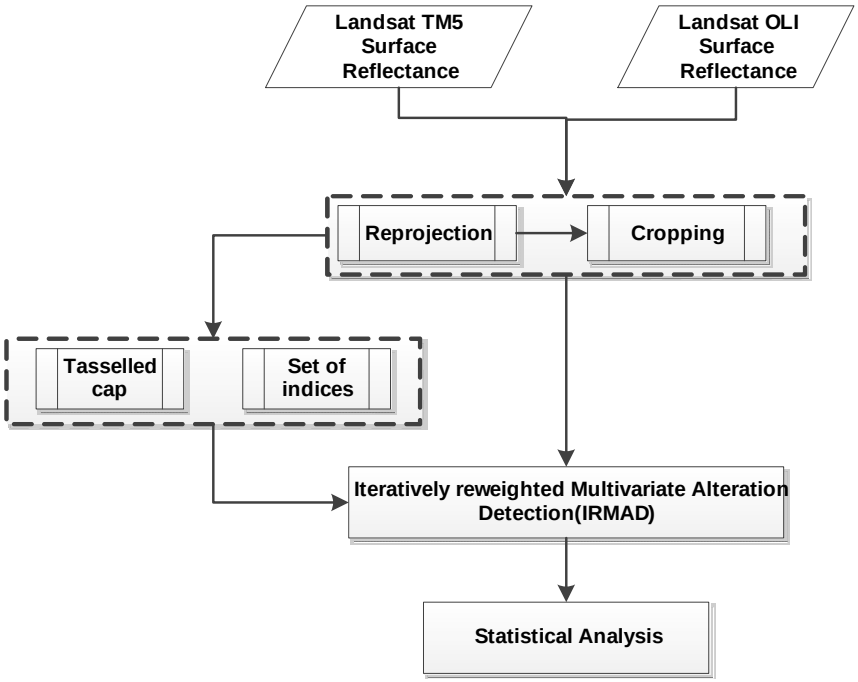

Figure 2. The process of analysis to compare the performance of transformed and untransformed images

4.2.1. Pre-processing and Spectral Transformation

Geotiff images of surface reflectance were extracted and reprojected from Universal Transverse Mercator (UTM) 48 South to Geographic projection, WGS 84 datum. The resulting images were cropped with a rectangular boundary to reduce image processing times (rectangle coordinates: upper left: 106.275, -6.555 and lower right: 107.150, -7.450). The TM images were stacked prior to transformation. The TC transformation for the Landsat TM5 images was based on Crist and Cicone (1984), while the TC transformation for Landsat 8 OLI was based on Baig et al. (2014). The TC transformation generates three features, namely brightness, greenness, and wetness. Therefore, the set of indices we studied in this experiment was selected to be comparable with TC features, namely the Brilliance Index (BI), Normalised Difference Vegetation Index (NDVI), and Normalised Differenced Water Index (NDWI), which were calculated as follows:

$$BI = \sqrt{\frac{[Red^2+Green^2]}{2}}\ ; \qquad NDVI = \frac{NIR\ \ -Red}{NIR\ \ +Red}; \qquad NDWI = \frac{NIR\ \ -SWIR}{NIR\ \ +SWIR} \tag{4}$$

4.2.2. IRMAD Comparison: Untransformed Surface Reflectance versus Tasseled Cap versus Set of Indices

IRMAD was performed with four pairs of images and comparisons were targeted to differentiate the effect of spectral transformations and type of sensors on change detection performance. Every pair of images was used to generate change maps directly from original surface reflectance or after being transformed into tasseled cap and the set of indices. Information about the image pairs is illustrated in Table 1. Each image pair spans six years between the first and second observations except for the pair composed of two OLI images, where the time span was only three years. The IRMAD process itself was evaluated to identify differences in how the techniques reached stable canonical correlations (i.e., number of iterations required). It is assumed that the stabilisation process is related to the quality of data, which is affected by any disturbances including geometric, atmospheric and radiometric differences, or the type of data being used.

Table 1. Pairs of Landsat images (path 122, row 65) used for IRMAD processing

Pairs	Date-1 (t0)	Date-2 (t1)	Sensors (% cloud cover)	Sun elevation of t0 and t1	Sun azimuth of t0 and t1
a	1991257	1997257	Both TM5 (10.8% and 0.4%)	52.5 and 54.6	74.3 and 73.6
b	2000250	2006250	Both TM5 (2.1% and 7.1%)	54.3 and 58.0	68.4 and 65.9
c	2007173	2013173	TM5 and OLI (2.9% and 20.1%)	47.6 and 48.9	42.8 and 40.9
d	2013221	2016230	Both OLI (11.5% and 11.9%)	53.3 and 54.7	50.9 and 54.5

Note: the date is in Julian date format YYYYDDD

5. RESULTS

5.1. Iterations Required to Reach Stable Canonical Correlation

Figures 3 and 4 show the canonical correlation coefficients at each iteration of the MAD process. Stable coefficients of canonical correlation were reached more quickly on the transformed data than the original surface reflectance. IRMAD processing of the TC or set of indices started to stabilise the coefficient after 15 iterations or less while the surface reflectance stabilised after 25 iterations. The surface reflectance result is similar to that found by Canty and Nielsen (2008) who concluded that convergence was usually reached between 20-30 iterations. Moreover, the period of observation, which affects the diversity of atmospheric, radiometric or systematic differences between images may affect iteration convergence. The Landsat TM5 1991-1997 image pair converged more rapidly than the later pair (2000-2006). This observation indicates that more disturbances obtruded on the later pair than the earlier one. There was a report of a severe floods occurred in Jakarta in 1996, 2002 and 2007 (Texier, 2008), indicating high rainfall at the corresponding years. It seems that worse atmospheric conditions were more likely to occur in the period of 2000-2006 than 1991-1997.

The different sensors also responded differently to IRMAD processing. Pairs composed only of Landsat TM5 data were less affected by disturbances. They required fewer iterations to reach stable canonical correlation in comparison to image pairs containing at least one Landsat 8 image. This pattern applied to both transformed and untransformed images. Examining each spectral band of the images, it appeared that the longer the wavelength, the quicker stability was reached. In this case, spectral bands 5 (NIR) and 7 (MIR) of Landsat TM5 reached stable canonical correlation more quickly than the visible bands (blue, green and red). While the values of the canonical correlation coefficients for the visible bands were still fluctuating after 15-25 iterations, bands 5 and 7 resulted in a stationary canonical correlation coefficient. The pattern applied for both the TM5 and OLI sensors.

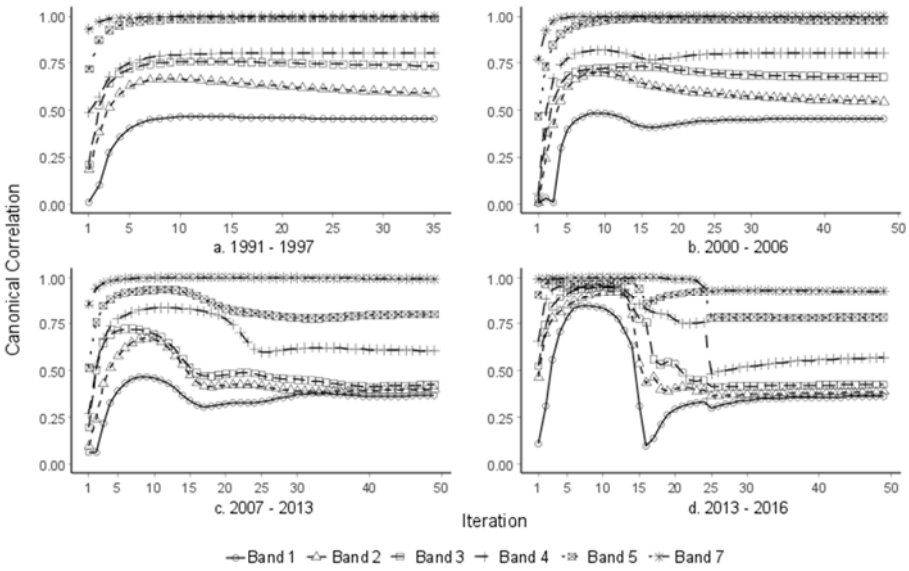

Figure 3. The coefficient of canonical correlation resulting from each iteration of IRMAD processing for four image pairs of LANDSAT surface reflectance (Band 1, Band 2, Band, 3, Band 4, Band 5 and Band 7).

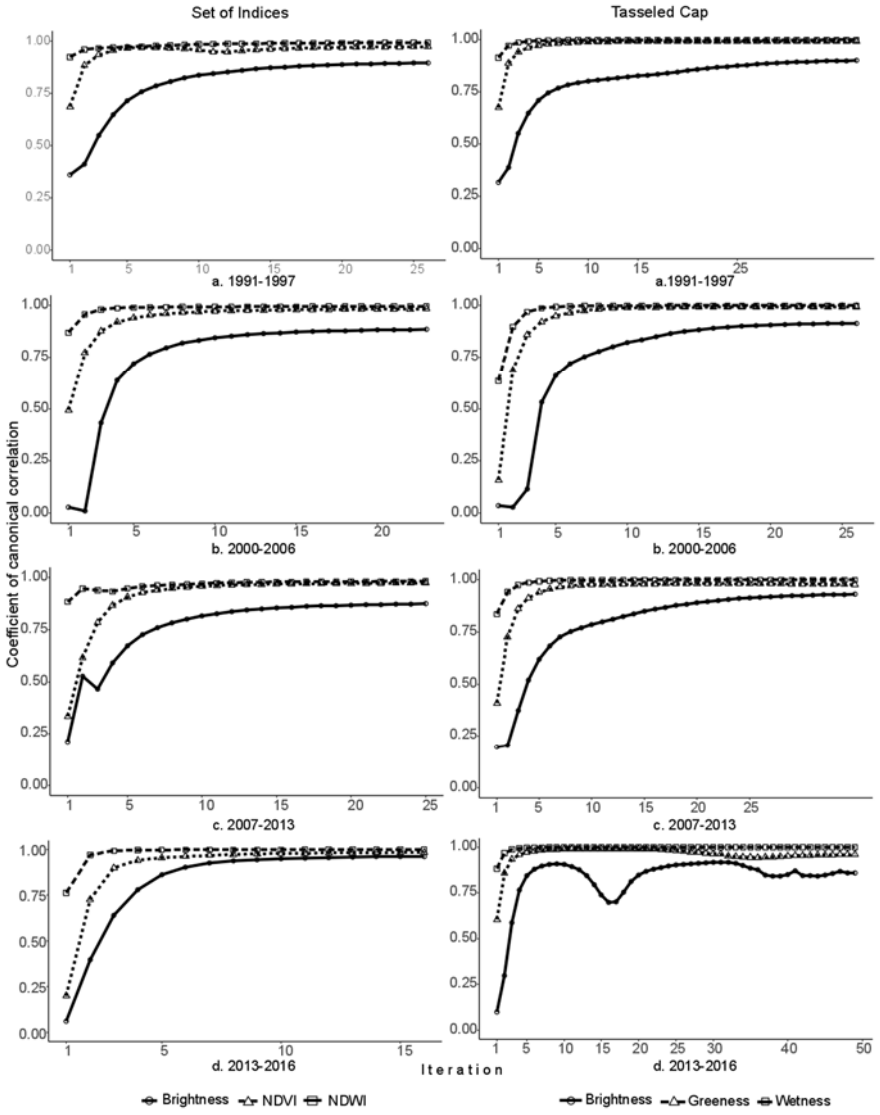

Figure 4. The coefficient of canonical correlation from each iteration of IRMAD processing of the tasseled cap and set of indices for four Landsat sensor pairs.

When image transformations were compared, the pattern shows that the set of indices seemed to reach stability more quickly than the TC image pairs. As stated by Crist (1985), TC is generally influenced by atmospheric conditions. In the experiment, the effect of atmospheric conditions on green spectral bands which are used to form the brightness and brilliance indices was observable, particularly in the generation of the coefficient of canonical correlations as seen in the OLI sensor.

5.2. IRMAD Statistics of Final Iteration

Statistics describing IRMAD variates show the distribution of changes and the characteristics of change on the transformed and untransformed image pairs. The change statistics are summarised in Table 2. Table 2 shows the value of MAD variates resulting from the different image pair comparisons for both untransformed and transformed image pairs. The number of MAD variates is the same as the number of variables input into the IRMAD transformation. Thus, Landsat surface reflectance image pairs produced six variates while tasselled cap or the set of indices generated three variates.

Table 2. IRMAD statistics derived from surface reflectance, tasselled cap and set of indices. a denotes image pair 1991–1997, b image pair 2000–2006, c image pair 2007–2013, d image pair 2013–2016

Parameters		Surface Reflectance				Tasselled cap				Indices			
	Spectral	a	b	c	d	a	b	c	d	a	b	c	d
Mean	B1	-0.36	-8.78	-6.17	-594.23	-0.829	-3.54	1.38	55.56	-0.9	-1.98	0.37	-0.39
	B2	-0.37	10.24	14.41	377.72	0.367	1.27	-0.62	20.72	1.62	-0.03	0.31	-1.1
	B3	-0.09	2.53	-3.26	-231.86	-0.045	0.11	0.16	-0.57	-0.2	-0.46	-0.28	-0.22
	B4	0.03	-2.01	11.8	-782.97								
	B5	-0.33	-1.56	7.96	-61.92								
	B6	-0.07	0	1.26	133.54								
Standard deviation	B1	11.37	135.84	35.27	276.74	7.354	51.39	17.99	160.35	4.84	26.07	6.41	12.56
	B2	6.85	61.29	46.65	245.45	2.415	16.61	8.32	47.52	4.98	4.53	3.41	12.1
	B3	7.51	37.5	39.61	214.71	0.376	1.85	0.72	4.99	1.12	6.12	4.75	2.31
	B4	3.77	30.51	24.73	350.44								
	B5	1.89	20.21	25.02	72.13								
	B6	0.37	1.73	6.95	67.84								
Eigenvalue	B1	99.99%	80.10%	45.20%	79.20%	100.00%	97.60%	94.30%	91.90%	100.00%	99.40%	78.80%	85.20%
(%)	B2	0.00%	14.70%	36.90%	13.50%	0.00%	1.20%	5.60%	8.00%	0.00%	0.50%	18.10%	13.80%
	B3	0.00%	3.80%	9.80%	5.40%	0.00%	0.40%	0.10%	0.10%	0.00%	0.10%	3.10%	1.10%
	B4	0.00%	1.20%	6.80%	0.90%								
	B5	0.00%	0.20%	0.90%	0.60%								
	B6	0.00%	0.00%	0.40%	0.40%								

The mean value of the MAD variates indicates the likelihood of change while the standard deviation suggests the spatial heterogeneity of the change. From the surface reflectance data, the mean of the MAD variates was smaller in TM5 than in OLI. The image pair containing two OLI images (d) resulted in the largest mean compared to the pairs containing two TM5 images (a, b) or the combination of TM5 and OLI (c). The standard deviation of the MAD variates indicates that the OLI image pair generated more heterogeneous change events than TM image pair. The heterogeneity may be due to sensor differences or the difference in atmospheric condition between those periods or the difference in actual changes.

Comparing the means of the MAD variates derived from the original surface reflectance (SR) and those of its transformations, it is clear that indices produced relatively smaller variates than SR or TC. The difference between MAD variates resulting from transformed and untransformed data was demonstrated in the OLI sensor. This result suggests that surface reflectance generates the biggest variates while indices produce the smallest. Comparing the transformation effect using the standard deviation (SD), it appears that the reduction of error from the first variate to the second in the set of indices was larger than in TC and seems more detectable in OLI than in TM. The SD that resulted from SR in the OLI sensor was 276, and TC transformation resulted in a value of 160, whereas the set of indices had a value of only 12. The standard deviation also decreased for the transformations of TM sensor images, but with a smaller reduction (see pair 1991–1997 or 2000–2006).

As the eigenvalue represents the variability of data, the value can be denoted in its proportional variance. In general, the eigenvalue of the MAD variates is ordered by decreasing variance (Table 2). The proportion of variance explained by the first MAD variate for surface reflectance tends to be smaller than for the transformed images. The first component (variate) usually represents the biggest variance of data, and indicate a condition that widely affects images. By comparing the distribution of change from the proportion of eigenvalue of MAD variates, it appears that TC generates the biggest common distribution in the first MAD variate for all data pairs. This means that the common 'changed' proportion would likely be greater in TC than untransformed SR or the set of indices. In contrast, specific change occurrences may be greater in SR and the set of indices.

6. CONCLUSION

The experiment demonstrates that transforming surface reflectance into TC or a set of indices may accelerate the stabilisation of the canonical correlation in the IRMAD process. However, careful examination of the proportion of cloud cover and the difference of illumination between data pairs is required. Users should be aware of this condition that might affect the result of the change detection. The number of iterations required to reach stable canonical correlation seems to be affected not only by transformation type and temporary atmospheric conditions, but also by the type of sensor and the reflectance wavelength. Indeed, the higher wavelengths required fewer iterations to reach the stationary canonical correlation compared to the visible bands, since they are not being affected by surface moisture.

It appears that the result of MAD variates representing the change was influenced by the transformations. It emerges that transformation is essential for time series analysis of images from the OLI sensor whereas it might be less important for TM images. OLI appears to result in a bigger mean difference and heterogeneous MAD variates compared to TM. However, employing surface reflectance of OLI might not yield a distinctive change. A direct comparison of different sensors within a similar period is required to prove that the type of sensor influences change identification.

These initial results require further examination, in terms of the accuracy of the change detection maps as well as identification of the driving forces behind change processes. Ground truth data, official maps and information from respected institutions or high spatial resolution imagery from Google Earth may assist in this process.

7. ACKNOWLEDGEMENT

This research was supported by The Australia Awards Scholarship to the first author and by UNSW Australia through UIPA scholarship to the last author. We would like to thank our assistants for their help during field surveys.

REFERENCES

Alaibakhsh, M., Emelyanova, I., Barron, O., Mohyeddin, A. and Khiadani, M., 2015. Multivariate detection and attribution of land-cover changes in the Central Pilbara, Western Australia. International Journal of Remote Sensing, 36(10), pp. 2599-2621.

Ayoub, F., Leprince, S. and Avouac, J.-P., 2009. Co-registration and correlation of aerial photographs for ground deformation measurements. ISPRS Journal of Photogrammetry and Remote Sensing, 64(6), pp. 551-560.

Baig, M.H.A., Zhang, L., Shuai, T. and Tong, Q., 2014. Derivation of a tasselled cap transformation based on Landsat 8 at-satellite reflectance. Remote Sensing Letters, 5(5), pp. 423-431.

Bernardo, N., Watanabe, F., Rodrigues, T. and Alcântara, E., 2016. An investigation into the effectiveness of relative and absolute atmospheric correction for retrieval the TSM concentration in inland waters. Modeling Earth Systems and Environment, 2(3), pp. 114.

Canty, M.J. and Nielsen, A.A., 2008. Automatic radiometric normalization of multitemporal satellite imagery with the iteratively re-weighted MAD transformation. Remote Sensing of Environment, 112(3), pp. 1025-1036.

Coppin, P.R. and Bauer, M.E., 1996. Digital change detection in forest ecosystems with remote sensing imagery. Remote sensing reviews, 13(3-4), pp. 207-234.

Crist, E.P., 1985. A TM tasseled cap equivalent transformation for reflectance factor data. Remote Sensing of Environment, 17(3), pp. 301-306.

Crist, E.P. and Cicone, R.C., 1984. A physically-based transformation of Thematic Mapper data---The TM Tasseled Cap. IEEE Transactions on Geoscience and Remote sensing(3), pp. 256-263.

Deng, J.S., Wang, K., Deng, Y.H. and Qi, G.J., 2008. PCA□based land□use change detection and analysis using multitemporal and multisensor satellite data. International Journal of Remote Sensing, 29(16), pp. 4823-4838.

Doxani, G., Karantzalos, K. and Tsakiri-Strati, M., 2012. Monitoring urban changes based on scale-space filtering and object-oriented classification. International Journal of Applied Earth Observation and Geoinformation, 15(1), pp. 38-48.

Du, Y., Teillet, P.M. and Cihlar, J., 2002. Radiometric normalization of multitemporal high-resolution satellite images with quality control for land cover change detection. Remote Sensing of Environment, 82(1), pp. 123-134.

Fiorella, M. and Ripple, W.J., 1993. Analysis of conifer forest regeneration using Landsat thematic mapper data. Photogrammetric Engineering and Remote Sensing, 59(9), pp. 1383-1388.

Gallo, K.P. and Tarpley, J.D., 1996. The comparison of vegetation index and surface temperature composites for urban heat-island analysis. International Journal of Remote Sensing, 17(15), pp. 3071-3076.

Gong, J., Sui, H., Ma, G. and Zhou, Q., 2008. A review of multi-temporal remote sensing data change detection algorithms. The International Archives of the Photogrammetry, Remote Sensing and Spatial Information Sciences, 37(B7), pp. 757-762.

Gong, M., Zhang, P., Su, L. and Liu, J., 2016. Coupled Dictionary Learning for Change Detection From Multisource Data. IEEE Transactions on Geoscience and Remote Sensing, 54(12), pp. 7077-7091.

Homer, C., Huang, C., Yang, L., Wylie, B. and Coan, M., 2004. Development of a 2001 National Land-Cover Database for the United States. Photogrammetric Engineering and Remote Sensing, 70(7), pp. 829-840.

Huang, C., Wylie, B., Yang, L., Homer, C. and Zylstra, G., 2002. Derivation of a tasselled cap transformation based on Landsat 7 at-satellite reflectance. International Journal of Remote Sensing, 23(8), pp. 1741-1748.

Huete, A.R., 2012. Vegetation Indices, Remote Sensing and Forest Monitoring. Geography Compass, 6(9), pp. 513-532.

Kauth, R.J. and Thomas, G., 1976. The tasselled cap--a graphic description of the spectral-temporal development of agricultural crops as seen by Landsat, LARS Symposia, pp. 159.

Lambin, E.F. and Ehrlich, D., 1997. Land-cover changes in sub-Saharan Africa (1982-1991): Application of a change index based on remotely sensed surface temperature and vegetation indices at a continental scale. Remote Sensing of Environment, 61(2), pp. 181-200.

Leprince, S., Barbot, S., Ayoub, F. and Avouac, J.P., 2007. Automatic and precise orthorectification, coregistration, and subpixel correlation of satellite images, application to ground deformation measurements. IEEE Transactions on Geoscience and Remote Sensing, 45(6), pp. 1529-1558.

Liang, S., Fang, H. and Chen, M., 2001. Atmospheric correction of Landsat ETM+ land surface imagery. I. Methods. IEEE Transactions on Geoscience and Remote Sensing, 39(11), pp. 2490-2498.

Lobser, S.E. and Cohen, W.B., 2007. MODIS tasselled cap: land cover characteristics expressed through transformed MODIS data. International Journal of Remote Sensing, 28(22), pp. 5079-5101.

Lunetta, R.S., Johnson, D.M., Lyon, J.G. and Crotwell, J., 2004. Impacts of imagery temporal frequency on land-cover change detection monitoring. Remote Sensing of Environment, 89(4), pp. 444-454.

Marpu, P.R., Gamba, P. and Canty, M.J., 2011. Improving change detection results of ir-mad by eliminating strong changes. IEEE Geoscience and Remote Sensing Letters, 8(4), pp. 799-803.

McFeeters, S.K., 1996. The use of the normalized difference water index (NDWI) in the delineation of open water features. International Journal of Remote Sensing, 17(7), pp. 1425-1432.

Milne, A.K., 1988. Change Direction Analysis Using Landsat Imagery: A Review Of Methodology, Geoscience and Remote Sensing Symposium, 1988. IGARSS '88. Remote Sensing: Moving Toward the 21st Century., International, pp. 541-544.

Nielsen, A.A., 2007. The regularized iteratively reweighted MAD method for change detection in multi- and hyperspectral data. IEEE Transactions on Image Processing, 16(2), pp. 463-478.

Nielsen, A.A., Conradsen, K. and Simpson, J.J., 1998. Multivariate alteration detection (MAD) and MAF postprocessing in multispectral, bitemporal image data: New approaches to change detection studies. Remote Sensing of Environment, 64(1), pp. 1-19.

Schmidt, M., King, E.A. and McVicar, T.R., 2008. A method for operational calibration of AVHRR reflective time series data. Remote Sensing of Environment, 112(3), pp. 1117-1129.

Schroeder, T.A., Cohen, W.B., Song, C., Canty, M.J. and Yang, Z., 2006. Radiometric correction of multi-temporal Landsat data for characterization of early successional forest patterns in western Oregon. Remote Sensing of Environment, 103(1), pp. 16-26.

Seto, K.C. and Fragkias, M., 2005. Quantifying spatiotemporal patterns of urban land-use change in four cities of China with time series landscape metrics. Landscape Ecology, 20(7), pp. 871-888.

Singh, A.N., 1989. Review Article Digital change detection techniques using remotely-sensed data. International Journal of Remote Sensing, 10(6), pp. 989-1003.

Son, N.T., Thanh, B.X. and Da, C.T., 2016. Monitoring Mangrove Forest Changes from Multi-temporal Landsat Data in Can Gio Biosphere Reserve, Vietnam. Wetlands, 36(3), pp. 565-576.

Texier, P., 2008. Floods in Jakarta: when the extreme reveals daily structural constraints and mismanagement. Disaster Prevention and Management, 17(3), pp. 358-372.

Townshend, J.R., Justice, C.O., Gurney, C. and McManus, J., 1992. The impact of misregistration on change detection. IEEE Transactions on Geoscience and Remote Sensing, 30(5), pp. 1054-1060.

Van Niel, T.G. and McVicar, T.R., 2004. Current and potential uses of optical remote sensing in rice-based irrigation systems: a review. Australian Journal of Agricultural Research, 55(2), pp. 155-185.

Wang, B., Choi, S.K., Han, Y.K., Lee, S.K. and Choi, J.W., 2015. Application of IR-MAD using synthetically fused images for change detection in hyperspectral data. Remote Sensing Letters, 6(8), pp. 578-586.

Zha, Y., Gao, J. and Ni, S., 2003. Use of normalized difference built-up index in automatically mapping urban areas from TM imagery. International Journal of Remote Sensing, 24(3), pp. 583-594.